Conference Proceedings of the Society for Experimental Mechanics Series

Jay Carroll · Samantha Daly *Editors*

Fracture, Fatigue, Failure, and Damage Evolution, Volume 5

Proceedings of the 2014 Annual Conference on Experimental and Applied Mechanics

SEM

Springer

Conference Proceedings of the Society for Experimental Mechanics Series

Series Editor

Tom Proulx
Society for Experimental Mechanics, Inc.,
Bethel, CT, USA

For further volumes:
http://www.springer.com/series/8922

Jay Carroll • Samantha Daly
Editors

Fracture, Fatigue, Failure, and Damage Evolution, Volume 5

Proceedings of the 2014 Annual Conference on Experimental and Applied Mechanics

Springer

Editors
Jay Carroll
Sandia National Laboratories
Albuquerque, NM, USA

Samantha Daly
University of Michigan
Ann Arbor, MI, USA

ISSN 2191-5644 ISSN 2191-5652 (electronic)
ISBN 978-3-319-06976-0 ISBN 978-3-319-06977-7 (eBook)
DOI 10.1007/978-3-319-06977-7
Springer Cham Heidelberg New York Dordrecht London

Library of Congress Control Number: 2014944551

Printed on acid-free paper

Springer is part of Springer Science+Business Media (www.springer.com)

Preface

Fracture, Fatigue, Failure and Damage Evolution, Volume 5: Proceedings of the 2014 Annual Conference on Experimental and Applied Mechanics represents one of eight volumes of technical papers presented at the 2014 SEM Annual Conference & Exposition on Experimental and Applied Mechanics organized by the Society for Experimental Mechanics and held in Greenville, SC, June 2–5, 2014. The complete Proceedings also includes volumes on: *Dynamic Behavior of Materials*; *Challenges in Mechanics of Time-Dependent Materials*; *Advancement of Optical Methods in Experimental Mechanics*; *Mechanics of Biological Systems and Materials*; *MEMS and Nanotechnology*; *Experimental Mechanics of Composite, Hybrid, and Multifunctional Materials*; *Experimental and Applied Mechanics*.

Each collection presents early findings from experimental and computational investigations on an important area within Experimental Mechanics, Fracture and Fatigue being one of these areas.

Fatigue and fracture are two of the most critical considerations in engineering design. Understanding and characterizing fatigue and fracture has remained as one of the primary focus areas of experimental mechanics for several decades. Advances in experimental techniques, such as digital image correlation, acoustic emissions, and electron microscopy, have allowed for deeper study of phenomena related to fatigue and fracture. This volume contains the results of investigations of several aspects of fatigue and fracture such as microstructural effects, the behavior of interfaces, the behavior of different and/or complex materials such as composites, and environmental and loading effects. The collection of experimental mechanics research included here represents another step toward solving the long-term challenges associated with fatigue and fracture.

Albuquerque, NM, USA — Jay D. Carroll
Ann Arbor, MI, USA — Samantha H. Daly

Contents

Chapter 1
Simulation of Arbitrary Mixed-Mode Crack Growth Using an Energy-Based Approach

B.R. Davis, P.A. Wawrzynek, and A.R. Ingraffea

Abstract A finite-element-based simulation technique is being developed to predict 3-D, arbitrary, non-planar evolution of mixed-mode crack growth. The approach combines a geometrically explicit crack front re-meshing scheme, and an energy-based growth formulation to predict extension magnitudes along the crack front. The technique also leverages a new 3-D mixed-mode energy release rate decomposition using the virtual crack extension (VCE) method. The energy-based crack growth formulation, previously implemented for planar crack growth, is extended to non-planar growth situations by employing a basis-function approach to describe crack front extensions. Rather than determining point-by-point extensions, calculating a governing function alleviates numerical influences on the crack growth predictions. The simulation technique seeks to mitigate computationally biased crack growth, as found in prescribed and mesh dependent methods, for example.

Keywords Crack growth • Energy release rate • Mixed-mode • Virtual crack extension • Finite-element analysis

1.1 Introduction

Many finite-element-based techniques have been developed to simulate 3-D arbitrary crack growth in structural components. Crack growth problems become inherently more difficult when complex loadings induce mixed-mode behavior. The resulting crack front evolution could become curved and tortuous. Utilizing a fracture mechanics approach to predict such complicated crack shape advances requires three main components: (1) crack representation, (2) fracture parameter calculations, and (3) crack extension application.

Currently, the prominent techniques for simulating 3-D, mixed-mode, arbitrary crack growth include the extended finite element method (XFEM) [1–3], cohesive zone elements [4, 5], and explicit crack front re-meshing schemes [6–9]. Each approach has been well developed throughout the literature, but as articulated in [10], suffer from some form of computational bias or require input on the expected crack evolution. For example, cohesive zone element approaches predict crack paths that are governed by the element locations, shapes, sizes and orientations. In some cases, finite element meshes are designed to adhere to the expected growth pattern, contradicting the notion of arbitrary crack evolution by linking a numerical artifact (the finite element mesh) with a physical phenomenon (crack growth). Alternatively, XFEM and re-meshing schemes often rely on user-prescribed growth increments to advance the front.

The unique crack growth simulation technique developed in [10] utilizes a new energy-based formulation that allows for the direct calculation of point-by-point crack front extensions. The formulation is derived from an energy expansion that depends on the first order variation of the energy release rate. The variation of energy release rate, made readily available via the virtual crack extension (VCE) method, acts as an influence function relating changes in energy from load increments to changes in geometry along the crack front. This term provides a mechanics-based approach to extract explicit crack extensions, avoiding the need to supply user-prescribed magnitudes of advance. The technique also employs a geometrically explicit crack representation that is continually updated through re-meshing schemes. As a result, mesh biased growth

B.R. Davis (✉) • P.A. Wawrzynek • A.R. Ingraffea
School of Civil and Environmental Engineering, Cornell University, 638 Rhodes Hall, Ithaca, NY 14853, USA
e-mail: brd46@cornell.edu

J. Carroll and S. Daly (eds.), *Fracture, Fatigue, Failure, and Damage Evolution, Volume 5: Proceedings of the 2014 Annual Conference on Experimental and Applied Mechanics*, Conference Proceedings of the Society for Experimental Mechanics Series,
DOI 10.1007/978-3-319-06977-7_1,

is reduced, allowing for the crack front to evolve arbitrarily. This form of crack representation is not a limitation of the technique, but deemed more practical for development purposes. The energy-based formulation can certainly be used with XFEM crack representations, for example.

The implementation of the simulation technique described in [10] is limited to mode I, planar crack growth conditions. It is the objective of the current work to extend the technique to simulate mixed-mode and non-planar, 3-D crack front evolution. To generalize the approach, an updated toolset is required. The commercial FRANC3D fracture analysis software [11] is used to represent and re-mesh the evolving non-planar crack front geometries. A new 3-D, mixed-mode VCE implementation (submitted and under review for publication) is developed to calculate the necessary energy release rates along the crack front. Finally, in conjunction with a trajectory criterion, a new basis-function approach to calculate extensions along an arbitrary front is constructed. The basis-function approach seeks to address sensitivity challenges associated with using a local, point-by-point approach for non-planar growth predictions. The focus of this proceeding will demonstrate the current status of the toolset development.

The next section will provide background and a description of the new 3-D, mixed-mode VCE implementation. Note that the full formulation and derivation of the mixed-mode VCE method will be available in an upcoming publication. Two examples are presented to verify the VCE mixed-mode energy release rate calculations. The following section will introduce the crack growth formulation, and its augmentation with the new basis-function methodology.

1.2 The Mixed-Mode Virtual Crack Extension Method

The VCE method for calculating energy release rates (also known as the stiffness derivative method) was first introduced by Dixon and Pook [12], and Watwood [13], and further developed by Hellen [14] and Parks [15]. Early VCE calculations utilized finite perturbations of meshes to approximate the required stiffness derivatives. This finite difference approach often introduced geometric approximation and numerical truncation errors. Using variational principle theories, a direct integral approach simplified the VCE method and improved accuracy and efficiency by eliminating the need for finite perturbations [16, 17]. The advent of the variational approach also allowed for the calculation of higher-order derivatives of energy release rate, the salient feature of the current method. Hwang et al. [18] generalized the variational formulations for planar 3-D cracks. A symmetric/anti-symmetric approach to decompose energy release rates, first demonstrated for a 2-D VCE method by Ishikawa [19] and later extended to 3-D equivalent domain J-integrals by [20–22], is used in the new 3-D VCE implementation.

1.2.1 Virtual Crack Extension Formulation

Following the formulation from [18], the VCE method is derived from the expression for the potential energy, Π, of a finite element system:

$$\Pi = \frac{1}{2} u^T K u - u^T f, \tag{1.1}$$

where u, K, and f are the displacement vector, the stiffness matrix, and the applied force vector, respectively.

The energy release rate, G, at crack-front position i is defined as the negative variation of the potential energy with respect to a virtual, incremental, crack-front extension, δa, in the normal direction of the front at that position:

$$G_i \equiv -\frac{\delta \Pi}{\delta A_i} = -\frac{\delta \Pi}{\delta a_i \ell_i}. \tag{1.2}$$

In the 3-D sense, the virtual extension has an associated area, δA_i, comprised of a virtual extension, δa_i, and an effective width, ℓ_i. Applying the variation to the finite element expression for potential energy leads to the following form of the energy release rate:

$$G_i = -\frac{1}{\ell_i} \left(\frac{1}{2} u^T \frac{\delta K}{\delta a_i} u - u^T \frac{\delta f}{\delta a_i} \right). \tag{1.3}$$

For simplicity in the current implementation, it is assumed that applied forces, f, are not influenced by the virtual incremental extension, and therefore the variational force term, $\frac{\delta f}{\delta a_i}$, is zero. The simplification reduces Eq. 1.3 to:

$$G_i = -\frac{1}{\ell_i}\left(\frac{1}{2}u^T\frac{\delta K}{\delta a_i}u\right). \tag{1.4}$$

Note, if the virtual extensions alter the nature of the applied load (e.g. with crack-face pressures, thermal, and body-force loadings), the effect must be accounted for with the variational force term, $\frac{\delta f}{\delta a_i}$, and included throughout the formulation.

The expression for the first-order variation of the energy release rate with respect to incremental crack extension, δa_j, follows from Eq. 1.4:

$$\frac{\delta G_i}{\delta a_j} = -\frac{1}{\ell_i}\left(u^T\frac{\delta K}{\delta a_i}\frac{\delta u}{\delta a_j} + \frac{1}{2}u^T\frac{\delta^2 K}{\delta a_i \delta a_j}u\right). \tag{1.5}$$

Note that Eqs. 1.4 and 1.5 represent the total global formulations of the VCE expressions for the energy release rate and rate of energy release rate. The integration and calculations are performed in a global coordinate system.

1.2.2 3-D Mixed-Mode Virtual Crack Extension Formulation

From Eq. 1.4, the energy release rate is composed of the stiffness derivative and nodal displacements. The stiffness derivative is fracture-mode invariant, leaving the displacements near the crack front to be decomposed into mode I, II, and III components. Using a local crack front coordinate system for each position along the front and the symmetric/anti-symmetric field decomposition found in [20], the local displacement modal contributions are determined such that:

$$u = u_I + u_{II} + u_{III}. \tag{1.6}$$

The decomposed displacements from Eq. 1.6 are substituted into Eq. 1.4, yielding the following expression for total energy release rate at position i:

$$G_i = -\frac{1}{\ell_i}\left[\frac{1}{2}(u_I + u_{II} + u_{III})^T\frac{\delta K}{\delta a_i}_L(u_I + u_{II} + u_{III})\right]. \tag{1.7}$$

Note that the stiffness derivative is also calculated in the local crack-front coordinate system to maintain consistency, and is denoted by subscript L. Expanding Eq. 1.7 leads to the separation of the decomposed energy release rate modes:

$$G_i = -\frac{1}{\ell_i}\left[\begin{array}{l}\left(\frac{1}{2}{u_I}^T\frac{\delta K}{\delta a_i}_L u_I\right) + \left(\frac{1}{2}{u_{II}}^T\frac{\delta K}{\delta a_i}_L u_{II}\right) + \left(\frac{1}{2}{u_{III}}^T\frac{\delta K}{\delta a_i}_L u_{III}\right)\\ + \left({u_I}^T\frac{\delta K}{\delta a_i}_L u_{II}\right) + \left({u_{II}}^T\frac{\delta K}{\delta a_i}_L u_{III}\right) + \left(\frac{1}{2}{u_{III}}^T\frac{\delta K}{\delta a_i}_L u_I\right)\end{array}\right]. \tag{1.8}$$

Extending from Ishikawa's 2-D VCE mode decomposition [19], the mode I and II energy release rates are as follows:

$$G_{Ii} = -\frac{1}{\ell_i}\left(\frac{1}{2}{u_I}^T\frac{\delta K}{\delta a_i}_L u_I\right), \tag{1.9}$$

$$G_{IIi} = -\frac{1}{\ell_i}\left(\frac{1}{2}{u_{II}}^T\frac{\delta K}{\delta a_i}_L u_{II}\right). \tag{1.10}$$

The unique contribution of the current implementation is the inclusion of the mode III energy release rate distribution along the crack front. The remaining terms in Eq. 1.8, excluding Eqs. 1.9 and 1.10, comprise a pure mode III component, $\frac{1}{2}{u_{III}}^T \frac{\delta K}{\delta a_i}_L u_{III}$, and three modal-interaction coupling terms. Understanding the influence of the coupling-mode terms is critical in determining their respective contributions to the 3-D mixed-mode energy release rates. Consider the following coupling mode terms from Eq. 1.8:

$$G_{I/II_i} = -\frac{1}{\ell_i}\left({u_I}^T \frac{\delta K}{\delta a_i}_L u_{II}\right), \tag{1.11}$$

$$G_{II/III_i} = -\frac{1}{\ell_i}\left({u_{II}}^T \frac{\delta K}{\delta a_i}_L u_{III}\right), \tag{1.12}$$

$$G_{III/I_i} = -\frac{1}{\ell_i}\left({u_{III}}^T \frac{\delta K}{\delta a_i}_L u_I\right). \tag{1.13}$$

Using symmetric and anti-symmetric arguments, it can be shown and verified numerically that calculating the coupling terms in Eqs. 1.11 and 1.13 about a symmetric domain lead to a cancellation effect. The result is $G_{I/IIi} = G_{III/Ii} = 0$. However, Eq. 1.12 has an additive effect that results in $G_{II/IIIi} \neq 0$. The only contributing non-zero components to $G_{II/IIIi}$ are out-of-plane shear. Therefore, any addition to the total energy release rate from $G_{II/IIIi}$ must be a factor of the out-of-plane mode III energy release rate:

$$G_{III_i} = -\frac{1}{\ell_i}\left(\frac{1}{2}{u_{III}}^T \frac{\delta K}{\delta a_i}_L u_{III}\right) + G_{II/III_i}. \tag{1.14}$$

With the individual mixed-mode terms determined and the modal-interaction coupling terms accounted for, the VCE total energy release is successfully decomposed, satisfying the following summation:

$$G_i = G_{I_i} + G_{II_i} + G_{III_i}. \tag{1.15}$$

1.2.3 Numerical Examples

In this section two verification analyses are presented to demonstrate the accuracy of the new, 3-D, mixed-mode energy release rate implementation using the VCE method. The mixed-mode VCE results are compared with analytical and M-integral methods. Each model and crack front geometry is meshed using the FRANC3D software.

The first problem considered a 45°-inclined circular crack centrally embedded within a rectangular isotropic body, as shown in Fig. 1.1. The model geometry was appropriately sized to approximate crack behavior within an infinite body. Analytical expressions for the mixed-mode I/II/III stress intensity factors for an inclined penny crack under remote tension [23] are used as a reference solution.

The second numerical example is a half-penny-shaped surface crack in an isotropic cylindrical specimen [24, 25]. Figure 1.2 shows the global geometry and loading conditions that induce mode II/III behavior along the crack front. The local, in-plane geometry of the crack front is depicted in Fig. 1.2. The VCE energy release rate results are compared with M-integral calculations using the FRANC3D software.

Figures 1.3 and 1.4 display the mixed-mode and total energy release rate distributions calculated by the VCE implementation for each example. The results compare extremely well with the reference solutions. The average percent differences between the VCE and reference results are 0.11 % and 0.23 % for the inclined circular crack and the surface-cracked cylinder, respectively.

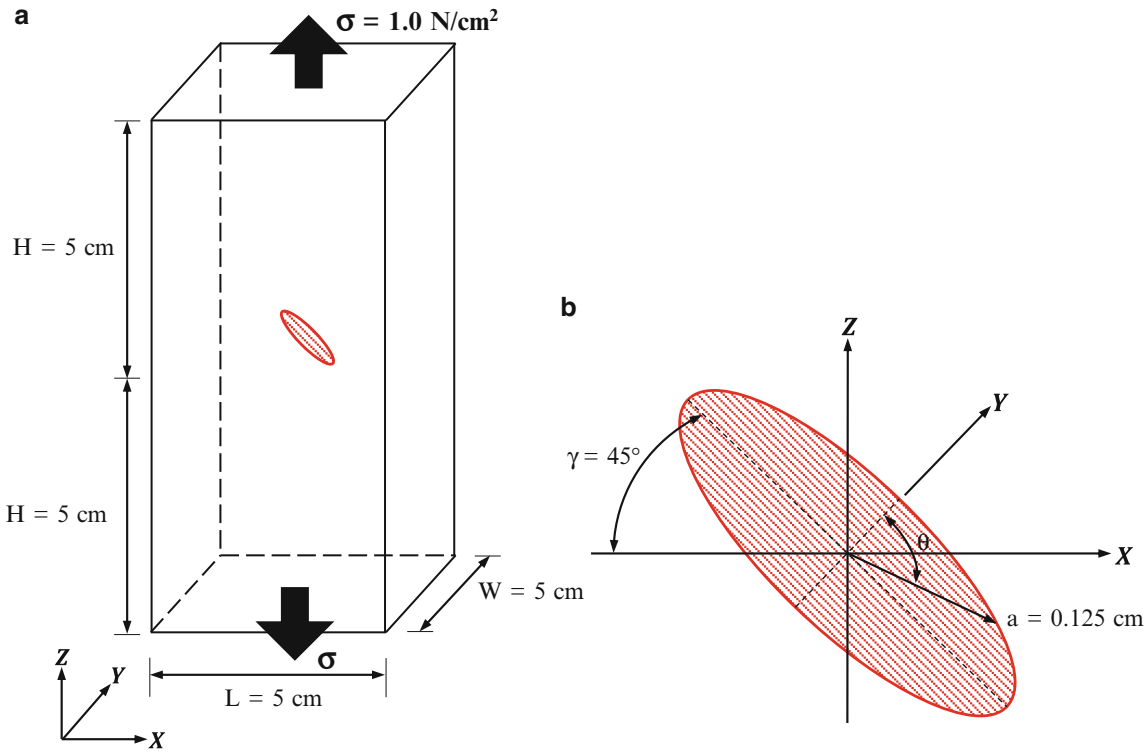

Fig. 1.1 Embedded inclined penny crack: (**a**) global geometry and loading conditions and (**b**) local crack-front geometry

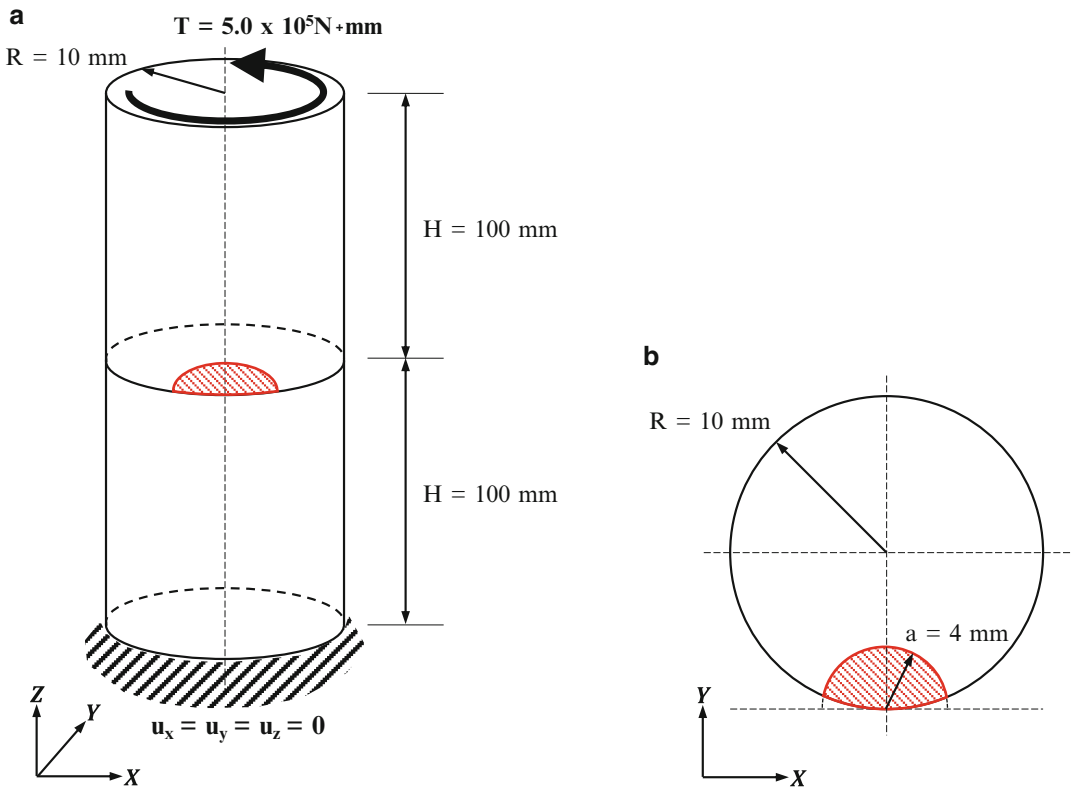

Fig. 1.2 Geometry and loading conditions for the penny-shaped surface crack in a cylindrical specimen: (**a**) global geometry and (**b**) local crack-plane geometry

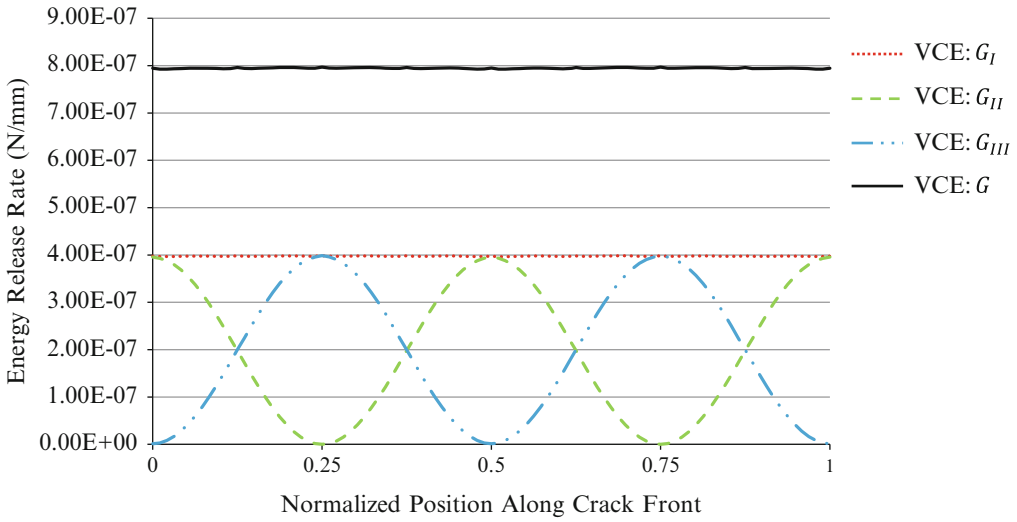

Fig. 1.3 Mixed-mode and total energy release rate distributions calculated by the VCE method for the inclined penny-crack specimen

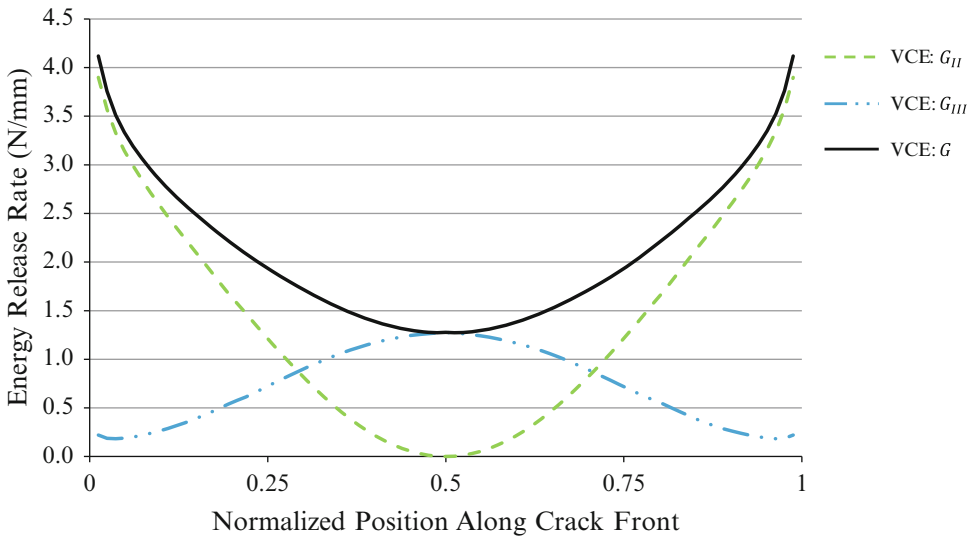

Fig. 1.4 Mixed-mode and total energy release rate distributions calculated by the VCE method for the surface-cracked cylindrical specimen

1.3 Crack Growth Formulation

The prediction of mixed-mode, non-planar crack front extensions requires two features. The first is a crack trajectory or kinking approach to determine the angle of advance for a position along the front. The second is a crack growth formulation to calculate the magnitudes of advances.

1.3.1 Crack Trajectory Criterion

For this work, a maximum critical energy release rate criterion is employed to obtain the extension angles [26]. For each position on the front, a series of virtual extensions that sweep radially along the local crack front normal are applied and energy release rates calculated. From this distribution the angle associated with the maximum energy release rate is chosen as the local position's extension angle. Certainly, other mixed-mode trajectory and kinking criteria can be used, such as maximum tensile stress and maximum shear stress.

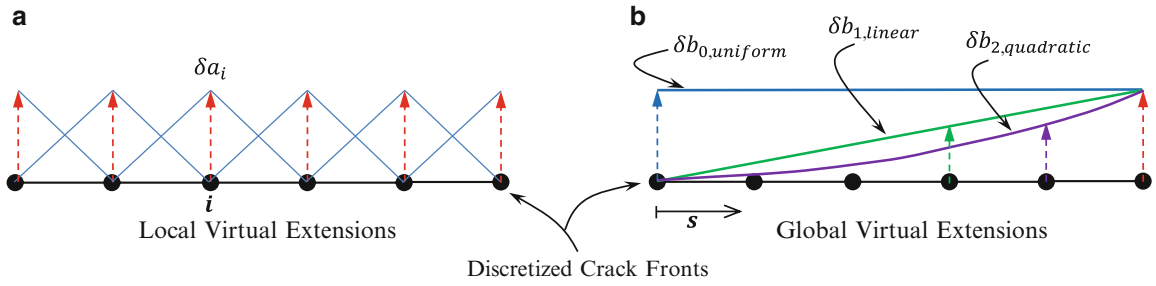

Fig. 1.5 Comparison between (**a**) local, point-by-point virtual crack extensions at position i, and (**b**) global basis-function virtual extensions along crack front length s

1.3.2 Basis-Function Growth Approach

The salient feature of this work is the modification of the crack growth formulation introduced in [10] to handle mixed-mode, non-planar growth situations. The planar growth formulation utilizes a balance equation extended from the first-order expansion of the energy release rate:

$$G_{ic} = G_i^0 + \frac{\delta G_i}{\delta P} \odot \Delta P_i + \frac{\delta G_i}{\delta a_j} \Delta a_j, \tag{1.16}$$

where G_{ic} is a critical energy release rate characterizing the material's resistance to crack growth; G_i^0 is the initial energy release rate prior to load increment ΔP_i; $\frac{\delta G_i}{\delta P} \odot \Delta P_i$ represents the energy contribution due to the applied load increment; $\frac{\delta G_i}{\delta a_j} \Delta a_j$ represents the energy contribution due to crack shape change. The $\frac{\delta G_i}{\delta a_j}$ term is the aforementioned rate of energy release rate parameter obtained through the VCE method that acts as an influence function relating energy changes to crack shape changes. By comparing energy contributions at an initial load level and after an applied load increment, Eq. 1.16 can be rearranged to directly obtain Δa_j, the point-by-point crack front extensions. Note that the critical energy release rate used for material toughness can be substituted with a mixed-mode fracture criterion or effective critical value and is not limited to a single toughness parameter.

Two major issues were encountered when attempting to apply the formulation for planar cracks described in [10] to non-planar growth situations. First, numerical sensitivities associated with the VCE calculations and the complicated front geometries were observed. These nominally insignificant undulations in energy release rate distributions along the front transpire through the growth formulation to create inconsistencies in the calculated crack front extension. These inconsistencies can accumulate and render the crack growth predictions nonsensical. Another concern is the accuracy of the VCE rate of energy release rate calculation. The suspect term within Eq. 1.5 is the variation of nodal displacements, $\frac{\delta u}{\delta a_j}$. The term, essentially, is obtained by applying a local virtual point perturbation at each position along the crack front and then obtaining a finite element solution. Similar to applying a nodal force in a standard finite element model, the local virtual point perturbation creates a region of high distortion near the perturbation.

To assuage both sources of error a new approach is applied to the VCE method. Rather than using local, point-by-point virtual extensions, δa_j, to calculate the rate of energy release rate, a basis-function approach is used. A set of linearly independent functions distributed along the crack front, δb_j, is used as virtual extensions. The expression for the rate of energy release rate now becomes:

$$\frac{\delta G_i}{\delta b_j} = -\frac{1}{\ell_i} \left(u^T \frac{\delta K}{\delta a_i} \frac{\delta u}{\delta b_j} + \frac{1}{2} u^T \frac{\delta^2 K}{\delta a_i \delta b_j} u \right). \tag{1.17}$$

The necessary calculations for each term are executed in a similar fashion to the standard local VCE approach. However, the second order virtual extensions are now globally applied across the crack front. Figure 1.5 shows a schematic demonstrating the difference between the local, point-by-point approach, and an example global, basis-function approach comprised of uniform, linear, and quadratic functions.

The augmented rate of energy release rate expression alters Eq. 1.16 so that the formulation calculates the coefficients of the basis functions that, when combined, represent a function for the predicted extensions along the crack front. The predicted extensions are then applied at the determined angle in the same manner described in the planar crack growth scheme.

The basis-function technique provides insulation against numerical noise by restricting the extension along the front to be smooth and continuous. The function characterizing the predicted growth mitigates the influence of the minor fluctuations in the energy release rate distributions on the individual front extensions. Additionally, by distributing the virtual extensions along the entire front, the point perturbation issue in the variation of nodal displacements is alleviated. This is analogous to applying a distributed force, i.e. a pressure, instead of nodal forces to avoid distortion in finite element results.

At this point no non-planar crack front evolution has been predicted using the basis-function approach. However, preliminary simulations have used the basis-function methodology to predict planar crack growth in a double cantilever beam specimen with applied displacement increments. The simulated uniform growth of the straight crack front compares well with analytical calculations and the local approach results from [10]. The predicted crack lengths have a relative difference of less than 1 %.

1.4 Conclusions

The presented work develops the toolset required for a new simulation technique to predict arbitrary mixed-mode crack growth. The technique relies on an explicit geometric representation of the crack through the meshing tools of FRANC3D. Fracture mechanics parameters of interest are calculated by a new 3-D mixed-mode VCE method. Finally, the energy-based crack growth formulation of [10] is modified through a novel basis-function approach to determine non-planar crack front extensions.

The development and implementation of the toolset is ongoing. Preliminary results show promise for mixed-mode and non-planar growth simulations. The VCE implementation is being extended to calculate energy release rates for anisotropic material systems, such as delaminations in composite laminates. The basis-function approach continues to be tested, and is being integrated within an incremental iterative crack growth simulation scheme for non-planar growth simulations.

Acknowledgements This work was funded by the NASA University Institutes Project under Grant NCC3-989, and the Cornell University Ross-Tetelman Fellowship in Civil and Environmental Engineering.

References

1. Areias PMA, Belytschko T (2005) Analysis of three-dimensional crack initiation and propagation using the extended finite element method. Int J Numer Methods Eng 63:760–788
2. Huang R, Sukumar N, Prévost J-H (2003) Modeling quasi-static crack growth with the extended finite element method. Part II: Numerical applications. Int J Solids Struct 40:7539–7552
3. Sukumar N, Chopp DL (2008) Three-dimensional non-planar crack growth by a coupled extended finite element and fast marching method. Int J Numer Methods Eng 76:727–748
4. Roy YA, Dodds RH (2001) Simulation of ductile crack growth in thin aluminum panels using 3-D surface cohesive elements. Int J Fract 110:21–45
5. Khoei AR, Moslemi H, Sharifi M (2012) Three-dimensional cohesive fracture modeling of non-planar crack growth using adaptive FE technique. Int J Solids Struct 49:2334–2348
6. Carter BJ, Wawrzynek PA, Ingraffea AR (2000) Automated 3-D crack growth simulation. Int J Numer Methods Eng 47:229–253
7. Moslemi H, Khoei AR (2009) 3D adaptive finite element modeling of non-planar curved crack growth using the weighted superconvergent patch recovery method. Eng Fract Mech 76:1703–1728
8. Gürses E, Miehe C (2009) A computational framework of three-dimensional configurational-force-driven brittle crack propagation. Comput Methods Appl Mech Eng 198:1413–1428
9. Maligno AR, Rajaratnam S, Leen SB, Williams EJ (2010) A three-dimensional (3D) numerical study of fatigue crack growth using remeshing techniques. Eng Fract Mech 77:94–111
10. Davis BR, Wawrzynek PA, Ingraffea AR (2014) 3-D simulation of arbitrary crack growth using an energy-based formulation—Part I: Planar growth. Eng Fract Mech 115:204–220
11. FRANC3D 6.0.5. Fracture Analysis Consultants, Inc., Ithaca, NY, USA (2013) www.francanalysis.com
12. Dixon J, Pook L (1969) Stress intensity factors calculated generally by the finite element technique. Nature 224:166–167
13. Watwood VB Jr (1969) The finite element method for prediction of crack behavior. Nucl Eng Des 11:323–332
14. Hellen TK (1975) On the method of virtual crack extensions. Int J Numer Methods Eng 9:187–207
15. Parks DM (1974) A stiffness derivative finite element technique for determination of crack tip stress intensity factors. Int J Fract 10:487–502
16. Haber RB, Koh HM (1985) Explicit expressions for energy release rates using virtual crack extensions. Int J Numer Methods Eng 21:301–315
17. Lin SC, Abel JF (1988) Variational approach for a new direct-integration form of the virtual crack extension method. Int J Fract 38:217–235
18. Hwang CG, Wawrzynek PA, Ingraffea AR (2001) On the virtual crack extension method for calculating the derivatives of energy release rates for a 3D planar crack of arbitrary shape under mode-I loading. Eng Fract Mech 68:925–947

19. Ishikawa H (1980) A finite element analysis of stress intensity factors for combined tensile and shear loading by only a virtual crack extension. Int J Fract 16:243–246
20. Nikishkov GP, Atluri SN (1987) Calculation of fracture mechanics parameters for an arbitrary three-dimensional crack, by the "equivalent domain integral" method. Int J Numer Methods Eng 24:1801–1821
21. Shivakumar KN, Raju IS (1992) An equivalent domain integral method for three-dimensional mixed-mode fracture problems. Engineering 42:935–959
22. Huber O, Nickel J, Kuhn G (1993) On the decomposition of the J-integral for 3D crack problems. Int J Fract 64:339–348
23. Kassir MK, Sih GC (1974) Three-dimensional crack problems, Mech. Fract. II. Noordhoff International Publishing, Leyden
24. Levan A, Royer J (1993) Part-circular surface cracks in round bars under tension, bending and twisting. Int J Fract 61:71–99
25. Ismail AE, Ariffin AK, Abdullah S, Ghazali MJ (2012) Stress intensity factors under combined tension and torsion loadings. Indian J Eng Mater Sci 19:5–16
26. Hussain MA, Pu SL, Underwood J (1974) Strain energy release rate for a crack under combined mode I and mode II. In: Fracture analysis. American Society for Testing and Materials, ASTM STP 560. pp 2–28

Chapter 2
Experimental and Predicted Crack Paths for Al-2024-T351 Under Mixed-Mode I/II Fatigue

E.E. Miller, M.A. Sutton, X. Deng, H. Watts, A.P. Reynolds, X. Ke, and H.W. Schreier

Abstract The aerospace industry has experience with a range of structural failures, oftentimes due to fatigue cracks in aircraft fuselage components that are exposed to relatively high stress levels during cyclic loading effects that lead to fatigue crack initiation at material defects and near stress concentrations. These aircraft components are under complex stress states. In this study, mixed mode I/II fatigue experiments and simulations are performed for an Arcan fixture and a 6.35 mm thick Al-2024-T351 specimen, a popular aerospace alloy. Experiments were performed for Arcan loading angles that gave rise to a range of Mode I/II crack tip conditions from $0 \leq \Delta KII/\Delta KI \leq \infty$. Measurements include the crack paths, loading cycles, and maximum and minimum loads for each loading angle. Simulations were performed using three-dimensional finite element analysis (3D-FEA) with 10-noded tetrahedral elements via the custom in-house FEA code, CRACK3D. While modeling the entire fixture-specimen geometry, a modified version of the virtual crack closure technique (VCCT) with automatic crack tip re-meshing and a maximum circumferential stress criterion was used to predict the direction of crack growth. Results indicate excellent agreement between experiments and simulations for the measured crack paths during the first several millimeters of crack extension.

Keywords Mixed mode • Fatigue • Arcan • Crack path • Modeling

2.1 Introduction

The aerospace industry has experience with a range of structural failures, oftentimes due to fatigue cracks in aircraft fuselage components that are exposed to relatively high stress levels during cyclic loading effects incurred during repeated take-off and landing events that lead to fatigue crack initiation at material defects and near stress concentrations. Numerous event over the last 30 years have been recorded where fatigue cracks in the fuselage have propagated to critical areas resulting the cabin opening up mid-flight and causing cabin depressurization along with numerous injuries and, in one case, death [1–3].

In fact, fatigue cracks are expected to form in the fuselage of modern airplanes due to repeated (a) pressurization and decompression of the cabin during every flight and (b) loading effects during take-off and landing. Thus, the propagation of cracks into critical joints continues to be an area of concern, especially since such propagation under complex stress states is not completely understood. Although procedures are currently in place to inspect and repair fatigue cracks, the ability to better predict how far a crack will propagate and in which direction it would grow when subjected to various loading conditions could save millions of dollars in premature inspection and repair, while also identifying the severity of an existing flaw in an aero-structure.

E.E. Miller (✉) • M.A. Sutton • X. Deng • H. Watts • A.P. Reynolds
Department of Mechanical Engineering, University of South Carolina, 300 Main St., Columbia, SC 29208, USA
e-mail: eileen.e.miller@boeing.com

X. Ke • H.W. Schreier
Correlated Solutions, Inc., 121 Dutchman Blvd, Columbia, SC 29063, USA

J. Carroll and S. Daly (eds.), *Fracture, Fatigue, Failure, and Damage Evolution, Volume 5: Proceedings of the 2014 Annual Conference on Experimental and Applied Mechanics*, Conference Proceedings of the Society for Experimental Mechanics Series,
DOI 10.1007/978-3-319-06977-7_2,

Crack propagation under Mode I loading is reasonably well understood [4]. Using a maximum circumferential stress (MCS) criterion, the predicted and actual crack trajectories during fatigue loading are perpendicular to the local $\sigma_{\theta\theta\ max}$ direction where $\sigma_{\theta\theta\ max}$ is the maximum circumferential stress ahead of the crack tip [5]. This direction nominally coincides with the loading direction when local conditions are not influenced by stress concentrations, material defections/inclusions, or other factors.

Now consider the case where a crack is under mixed-mode loading, that is, under any combination of two or more loading types. For the combination of Mode I and Mode II loading conditions, methods for obtaining a mixed-mode I/II stress state experimentally when applying uniaxial tensile loading include (a) use of kinked cracks, (b) use of cracks propagating away from a hole, and (c) use of an Arcan fixture [6–15]. Independent mixed mode loading studies by both Zhang et al. [21] and Lopez-Crespo et al. [22] have used an Arcan fixture to statically load an existing crack for conditions in which an empirical solution for the stress intensity factor (SIF) exits [23]. While their experimental results were consistent with the empirical solution, the empirical solution has limitations, mainly being that the model can only be used for determining the kinking angle for the initial crack propagation event.

Gaylon et al. [6] performed fatigue tests using the Arcan fixture. In this study, the authors determined the crack growth trajectory for various degrees of mixed-mode I/II loading. The measured crack trajectories suggest that for all combinations of Mode I/II loading, the fatigue cracks propagate in a manner that was locally dominated by K_I, while no crack propagation occurred for the pure Mode II loading case. However, there was such large scatter in the experimental data that it is difficult to definitively identify the trends. One cause of the inconsistency in the results was determined to be the three pin loading configuration used by the authors. It was suggested that future studies use only one pin for fixing the Arcan fixture to the test stand [7]; the use of a single pin is consistent with the work of Amstutz, Boone and others at the University of South Carolina [8, 9, 10].

Chao et al. [8] used the Arcan fixture with the one-pin configuration to study fatigue crack propagation under various mixed-mode loading conditions. Crack trajectories were compared to stable tearing results obtained under mixed-mode monotonic loading conditions. It was observed that cracks under fatigue loading propagate in a local Mode I direction for all loading cases including pure Mode II, unlike Gaylon's results. In Chao's studies, the amount of crack growth in fatigue for $\Phi = 75°$ and 90° was quite small, indicating that the crack surfaces interfered after a small amount of crack extension and impeded further crack growth. For stable tearing, after Mode II loading becomes dominant, cracks in aluminum alloys tended to propagate in the local shear direction; that is, approximately parallel to the direction of the pre-crack. This transition from Mode I dominated crack growth to Mode II dominated crack growth under stable tearing conditions is consistent with results obtained by Amstutz et al. [9, 10]. In Amstutz's work, the authors used the Arcan fixture to study mixed Mode I/II stable tearing crack growth. The results show that for most loading cases, where $K_{II}/K_{I,} < 1$, the crack propagates under local Mode I conditions. However, as K_I approaches zero and K_{II}/K_I reaches a critical value ($\Phi = 75°$ and 90° for Al 2024-T351), the crack begins to grow in Mode II. While this study included crack propagation, stable tearing occurs outside of the linear elastic range, and results suggest that the Mode II component has different effects in the linear elastic range than it does under elastic-plastic conditions.

Boljanovic [11] performed finite element analysis to model the results of Gaylon et al. The crack trajectories were simulated using MSC [12] a step-by-step method while applying the maximum circumferential stress (MCS) criterion to predict crack trajectory. Results of Boljanovic's work agree with Gaylon's experimental crack paths. However, the SIFs were not obtained at each step using the local crack tip field data, but were determined analytically after the simulation was performed since the step-by-step method of crack path prediction is quite time consuming. It is unclear if the analytical solution for the SIFs accounted for curvilinear crack paths.

The objective of the current study is to (a) perform experiments and measure the crack path and (b) perform simulations and predict the fatigue crack path in an aerospace aluminum alloy undergoing applied, far-field mixed-mode I/II conditions. The Arcan fixture will be utilized to achieve far-field mixed-mode I/II conditions in 6.35 mm thick Al-2024-T351 specimens. Crack paths, cycle count, and maximum and minimum loads will be measured during experiments, with loading ranging from $0 \leq K_{II}/K_I \leq \infty$. Simulations will then be performed using 3D-FEA. Crack trajectories will be predicted using virtual crack closure techniques (VCCT) and a MCS criterion. Local re-meshing will be used to extend the crack. The whole fixture and specimen will be modeled using 10-noded tetrahedral elements. Predicted crack paths will be compared to the results obtained experimentally, and the results will be discussed.

2.2 Experimental Work

2.2.1 Fixture and Specimen

The Arcan was used to achieve mixed-mode I/II loading for discrete values of K_{II}/K_I in the range $0 \leq K_{II}/K_I \leq \infty$. With loading angle Φ defined as shown in Fig. 2.1, the $\Phi = 0°$ pin holes correspond to nominally Mode I crack conditions and the $\Phi = 90°$ pin holes represent nominally Mode II crack loading conditions. As shown in Fig. 2.1, each butterfly-shaped specimen is 224.28 mm tall, 275.30 mm wide at the top and bottom of the specimen and 6.35 mm thick. Each specimen is manufactured from Al-2024-T351 to form an LT orientation crack configuration (crack is along the transverse direction (T) and perpendicular to the rolling direction (L) in the aluminum specimen) [13] with Young's modulus $= 7.11 \times 10^{10}$ Pa and Poisson's ratio $= 0.33$. A jeweler's saw blade, size 0/6, was used to create an initial through-thickness edge notch 6.35 mm long in the width direction on the left side of the specimen in the vertical center. The front and back surfaces of the specimens were sanded with 600 grit sand paper before final sanding with 800 grit sandpaper to remove small surface defects. Metal polish was used to create a mirror finish on the surfaces for visually tracking crack tip progression during the experiment.

2.2.2 Set Up

A 50 kip (227 kN) servo-hydraulic Material Test System (MTS) controlled by TestStar II software was used to apply tensile loads to the Arcan fixture and specimen. Figure 2.2 shows the set up without the microscope objectives. The backing plate (not visible in Fig. 2.2) is attached to the top and bottom pieces of the Arcan fixture and is oriented at 45°.

During testing, the crack tip was tracked using the microscope objective and the slide apparatus. The objective is attached to the dual slide apparatus shown in Fig. 2.3. The apparatus consists of (a) a single, horizontally mounted manual screw driven slide manufactured by Velmex with a digital caliper to provide a metric positional measurement, (b) a second vertically-oriented Velmex slide with digital caliper that was mounted to the horizontal slide. The microscope objective was then connected to the vertical slide. Both vertical and horizontal slides operate independently, allowing for horizontal and vertical measurements of the crack tip position during the fatigue process.

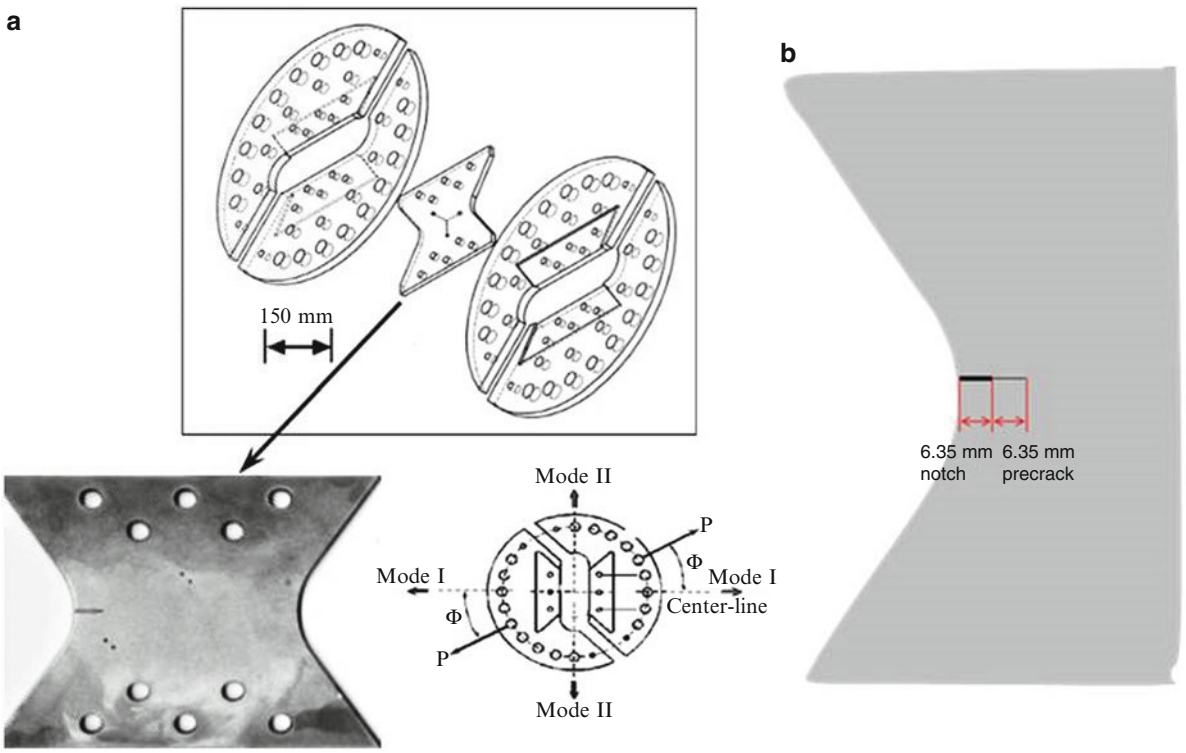

Fig. 2.1 (**a**) Mixed mode I/II Arcan test fixture and butterfly shaped test specimen. Angle $\Phi = 0°$ corresponds to far-field tension and $\Phi = 90°$ is far-field shear (**b**) diagram of notch and pre-crack

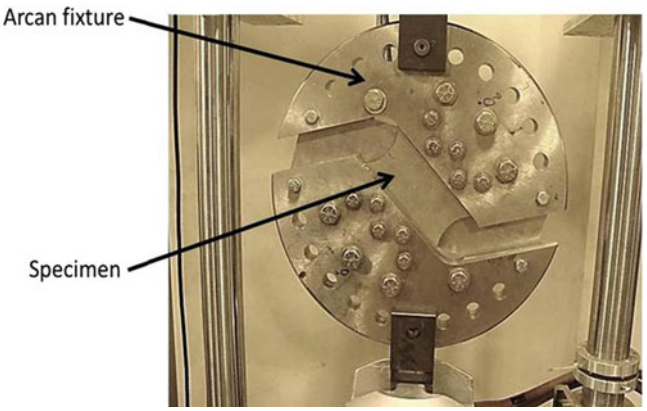

Fig. 2.2 Image of experimental set up

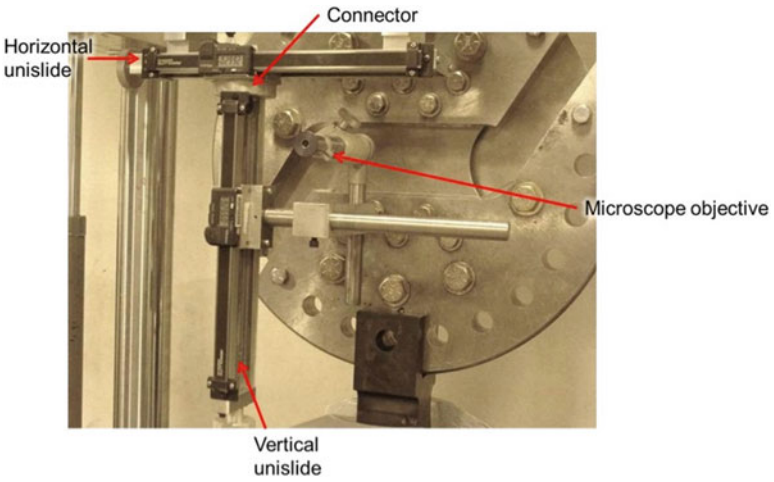

Fig. 2.3 Two degree-of-freedom slide apparatus

2.2.3 Load Prediction

Load shedding was performed to avoid the risk of initiating stable tearing or formation of a large plastic zone at the crack tip. Given that the empirical solution for the stress intensity factor was only valid for static loading and the traditional method of load prediction was going to be quite crude, a modified approach was taken. The goal of the modified approach was to keep ΔK constant in order to avoid excessive plasticity in the crack tip region, crack slanting, or crack tearing. Since the method for estimating the SIF was quite crude, and did not account for the various loading angles and resulting K_I and K_{II} values, it was determined that following Paris' Law for the material was a more accurate method of crack growth control for ΔK_{eq} which is defined as follows [14];

$$\Delta K_{eq} = \gamma \Delta K_I + (1-\gamma)\sqrt{(\Delta K_I)^2 + \gamma_1(\Delta K_{II})^2 + \gamma_2(\Delta K_{III})^2} \tag{2.1}$$

where γ, γ_1, and γ_2 are parameters to be defined. Using ΔK_{eq} and assuming that there is no crack closure effect, the crack growth rate can be determined using Paris' Law. That is, the authors opted to maintain the same crack growth rate throughout the experiment.

From the previous test data, it was determined that a crack growth rate of $\approx 6 \times 10^{-5}$ mm/cycle was a safe rate to run the experiments and maintain nominally linear elastic conditions. A loading ratio R = 0.4 was chosen for the experiment. This crack growth rate was maintained by allowing the crack to grow until the rate increased to $\approx 8 \times 10^{-5}$ mm/cycle. The load was then dropped by approximately 5 %, resulting in a crack growth rate of $\approx 4 \times 10^{-5}$ mm/cycle. This process was repeated to maintain an average crack growth rate of $\approx 6 \times 10^{-5}$ mm/cycle and therefore maintain a constant average ΔK_{eq} during the experiment.

2.2.4 Procedure

Initially, the specimen is oriented to be in the Mode I configuration. The specimens were fatigue pre-cracked an additional 6.35 mm for a total crack length of 12.7 mm. Fatigue loading was applied in force control at 10 Hz. Then the fixture was rotated in the test stand to the appropriate loading angle. A total of six experiments were performed at loading angles $\Phi = 15°$, 30°, 45°, 60°, 75°, and 90°, with $\Phi = 90°$ degrees being nominally Mode II crack loading. For the loading cases $\Phi = 15°$, 30°, and 45°, the one degree of freedom slide apparatus was used for tracking the crack tip. The two degree of freedom slide apparatus was built and used to track the crack tip for $\Phi = 60°$, 75°, and 90°. Again, fatigue loading at 10 Hz was applied in force control. The crack tip position was measured approximately every 5,000–20,000 cycles.

2.3 Theoretical Work

2.3.1 Approach

CRACK3D is a three-dimensional finite element code first developed by the University of South Carolina and later jointly by the University of South Carolina and Correlated Solutions, Inc. It is capable of simulating elastic-plastic stable tearing crack extension and linear-elastic fatigue crack propagation, both with curved crack fronts and curvilinear crack paths for mixed-mode conditions. Two methods of crack growth simulations are available: nodal release and local re-meshing. In the case that the crack path is to be predicted, local re-meshing is used to extend the crack [15, 19, 20]. For the case of fatigue crack propagation, there are three steps to crack growth predictions: (1) will the crack grow? (2) in what direction will it grow? (3) how far will it extend for a certain number of loading cycles or how many loading cycles will be required to extend the crack by a certain amount?

For determining if the crack will propagate, $\Delta K > \Delta K_{TH}$ must be true. CRACK3D can be used to evaluate ΔK, which can be used to check if $\Delta K > \Delta K_{TH}$ is satisfied. Once this crack growth criterion is met, CRACK3D can be used to simulate the crack growth process and predict (a) the direction of crack growth and (b) the variations of stress intensity factors with the amount of crack growth, which can be used to predict the number of loading cycles as a function of the amount of crack growth. In CRACK3D the determination of stress intensity factors is done using the method of three-dimensional virtual crack closure technique (3D-VCCT) [5, 15, 16, 19, 20], which is based on the approach of the strain energy release rate [17]. Once the SIFs for the maximum applied load are predicted using the VCCT, the direction in which the crack will propagate is predicted using Maximum Circumferential Stress Criterion [5]. A fatigue crack growth rate model, such as the Paris' Law, is used to determine how many cycles it will take for the crack to grow the amount of crack extension chosen by the user [18].

To apply the VCCT in crack growth simulations using the local re-meshing option (instead of the nodal release option), the local mesh immediately ahead and behind the crack front must be properly structured, so that the local mesh immediately behind the crack front can be viewed as being shifted by one element size from the local mesh immediately ahead of the crack front. Therefore, once crack growth is determined to occur along a certain direction with a certain increment, the new mesh around the new crack front is generated such that there is a structured mesh (within a local re-meshing zone around the new crack front) with equal number of elements behind the crack front and ahead of the crack front [15, 19, 20].

2.3.2 Geometry, Mesh Generation and Boundary Conditions

The Arcan fixture and specimen were modeled as shown in Fig. 2.4. For simplicity, this fixture-specimen connection is approximated by a continuous bond at the fixture-specimen boundary. To this end, the bolts are not modeled and the fixture and specimen are treated as three solid regions with different thicknesses. An idealized through-thickness edge notch and pre-crack exactly 12.7 mm long was modeled as the initial crack in the exact geometric vertical center of the specimen and is perfectly horizontal into the width of the specimen. The volumes were then meshed with 10 noded tetrahedral elements.

For each loading angle, Φ, a set of lines (one on the top fixture and the other on the bottom fixture) corresponding to the center of the pins were created on the surface of the fixture model in the through-thickness direction. The boundary conditions were such that the displacement of the bottom line was set to zero in the x and y directions (u_x, and $u_y = 0$) and only the z displacement specified was of the center point on the bottom line ($u_z = 0$). The displacement of the corresponding

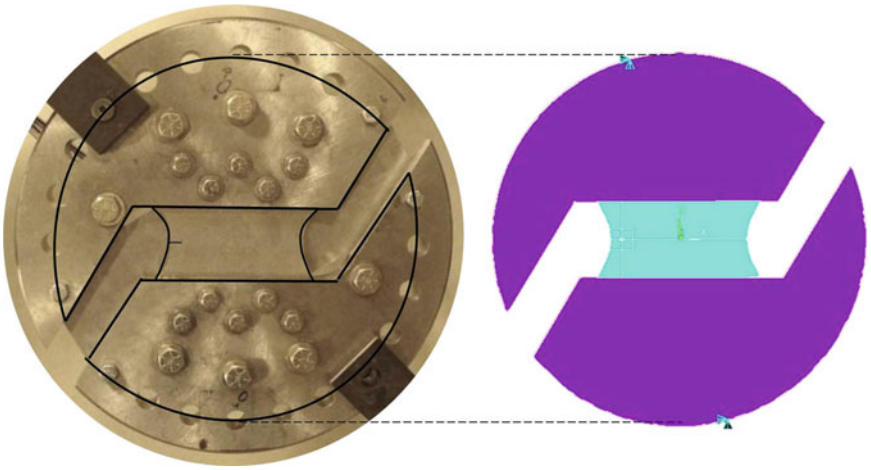

Fig. 2.4 Diagram of a picture of actual Arcan fixture and specimen (*left*) and image of finite element model geometry (*right*)

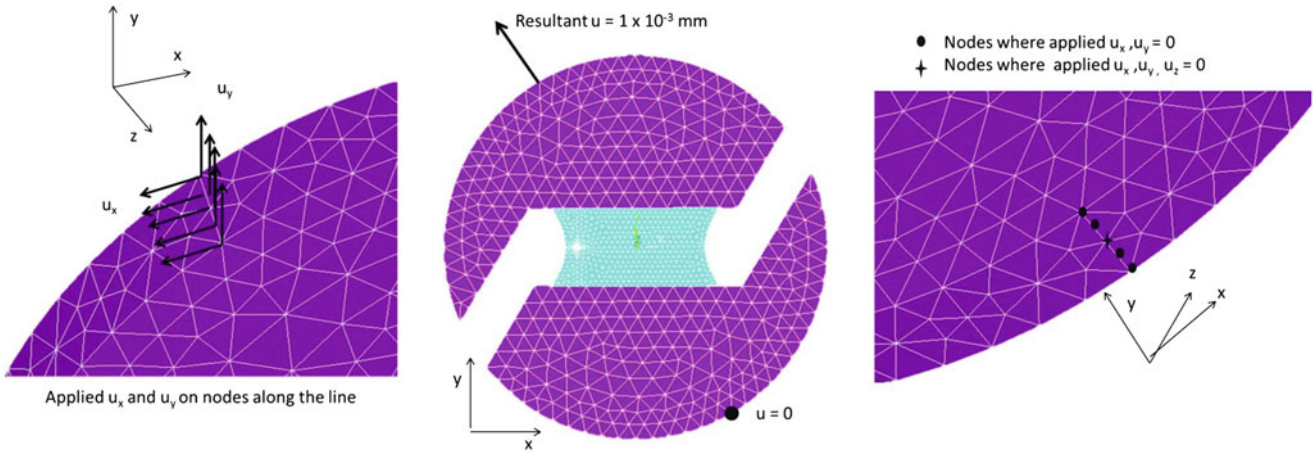

Fig. 2.5 Boundary conditions at $\Phi = 30°$

top line had a magnitude of 1×10^{-3} mm along the direction of loading, Φ, as shown in Fig. 3.7, which was decomposed into x and y components (Fig. 2.5).

2.4 Results

For loading cases 15°, 30°, 45°, and 60°, fatigue crack propagation occurred, and for loading cases 75° and 90°, no crack propagation occurred. The experimental and predicted crack paths are plotted in Fig. 2.6.

The ΔK_I and ΔK_{II} for each loading cases $\Phi = 15°, 30°, 45°$, and 60° are plotted along the crack length a in Figs. 2.7–2.10 respectively.

2.5 Discussion

Prior to discussing the results for the Arcan fatigue studies, it is important to note that benchmark studies have been performed, and it has been verified that CRACK3D is able to accurately predict the crack path for elastic plastic stable tearing using the Arcan fixture to achieve mixed-mode loading conditions using local re-meshing [9, 10, 15, 19, 20]. The direction of crack extension for stable tearing is predicted with a different criteria, crack opening displacement [9, 10, 15, 19, 20], while as discussed here, VCCT and MCS criterion are used in predicting the direction of fatigue crack propagation.

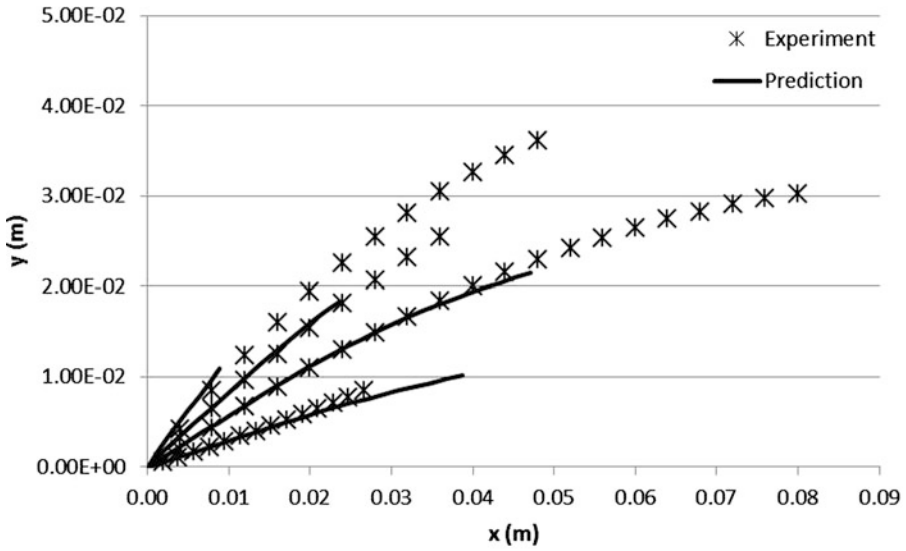

Fig. 2.6 Experimental and predicted crack paths

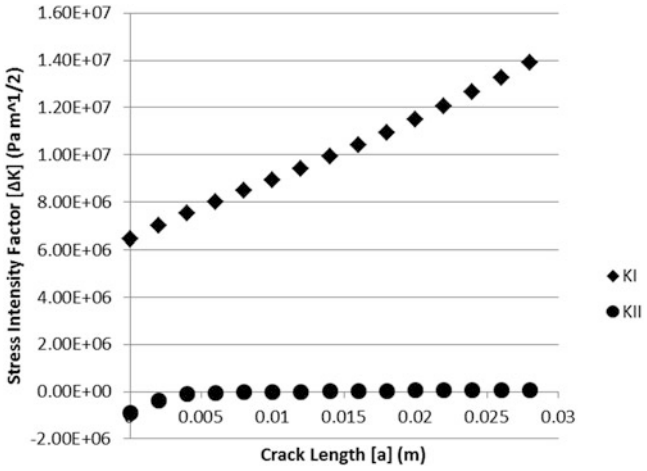

Fig. 2.7 Plot of ΔKI and ΔKII along the crack path for the 15°

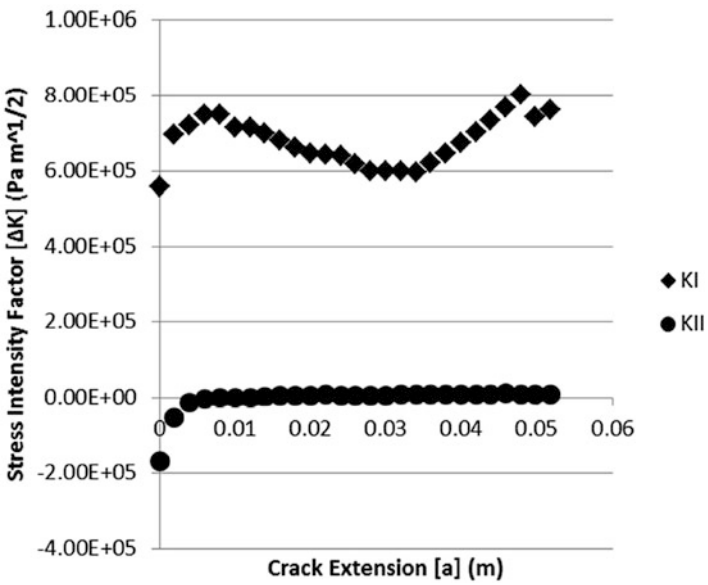

Fig. 2.8 Plot of ΔKI and ΔKII along the crack path for the 30°